Terahertz generation in plasmas using two-color laser pulses

Joseph Peñano,[1] Phillip Sprangle,[1] Bahman Hafizi,[2] Daniel Gordon,[1] and Philip Serafim[3]
[1]*Naval Research Laboratory, Plasma Physics Division, Washington, DC 20375, USA*
[2]*Icarus Research, Inc., Bethesda, Maryland, USA*
[3]*Northeastern University, Boston, Massachusetts, USA*
(Received 5 October 2009; published 26 February 2010)

We analyze the generation of terahertz radiation when an intense, short laser pulse is mixed with its frequency-doubled counterpart in plasma. The nonlinear coupling of the fundamental and the frequency-doubled laser pulses in plasma is shown to be characterized by a third order susceptibility which has a time dependence characteristic of the laser pulse durations. The terahertz generation process depends on the relative polarizations of the lasers and the terahertz frequency is $\omega \sim 1/\tau_L$, where τ_L is the laser pulse duration. Since the laser pulse duration is typically in the picosecond or subpicosecond regime the resulting radiation is in the terahertz or multiterahertz regime. To obtain the third order susceptibility we solve the plasma fluid equations correct to third order in the laser fields, including both the relativistic and ponderomotive force terms. The relativistic and ponderomotive contributions to the susceptibility nearly cancel in the absence of electron collisions. Therefore, in this terahertz generation mechanism collisional effects play a critical role. Consistent with recent experimental observations, our model shows that (1) the terahertz field amplitude is proportional to $I_1\sqrt{I_2}$, where I_1 and I_2 are the intensities of the fundamental and second harmonic laser pulses, respectively, (2) the terahertz emission is maximized when the polarization of the laser beams and the terahertz are aligned, (3) for typical experimental parameters, the emitted terahertz field amplitude is on the order of tens of kilovolts/cm with duration comparable to that of the drive laser pulses, and (4) the direction of terahertz emission depends sensitively on experimental parameters.

DOI: 10.1103/PhysRevE.81.026407 PACS number(s): 52.38.−r, 42.65.Re

I. INTRODUCTION

Terahertz radiation sources have a number of applications ranging from imaging and terahertz spectroscopy, to chemical and biological detection [1,2]. A variety of processes can be used to generate terahertz radiation. Terahertz sources include: multicolor laser photoionization processes in air [3–18], photoactivated semiconductor switches [19,20], as well as gyrotron-based sources [21,22].

Terahertz radiation in plasmas has been observed in various experiments employing two laser beams, one at the fundamental and the other at the second harmonic. These plasma-based sources of terahertz radiation have the advantage that they can be scaled to high peak powers. In the experiments of Xie, *et al.*, it was observed that the properties of the emitted terahertz radiation are consistent with four-wave mixing in a plasma, i.e., the terahertz energy is proportional to $I_1^2 I_2$ and the terahertz emission is maximized when the polarization of the laser beams and the terahertz are aligned [9].

A terahertz generation mechanism based on tunneling ionization of a gas by two-color laser fields has been proposed [10,11]. In this mechanism the ionized electrons acquire a nonzero drift velocity which results in a current density capable of generating terahertz radiation.

In this paper an alternative two-color terahertz generation mechanism, shown schematically in Fig. 1, is described and analyzed. In this mechanism the interaction of the two laser beams in a plasma leads to the generation of a nonlinear current density with a component that can drive radiation in the terahertz regime. The nonlinear current density in general has contributions from both ponderomotive forces and relativistic effects. For the parameters of interest, where collisions are important, the relativistic contribution is small compared with the ponderomotive contribution. We use the terahertz driving current to determine the electromagnetic field characteristics such as spectral intensity, electric field amplitude, energy, and directionality.

Our terahertz generation model is presented in Sec. II. We derive the terahertz driving current density which consists of ponderomotive and relativistic contributions and discuss the role of collisions. In Sec. III, we calculate the properties of the emitted terahertz radiation, i.e., the spectrum, spatial distribution, and total energy. Section IV presents numerical results and discusses them in relation to experimental findings, and Sec. V is a summary.

II. TERAHERTZ GENERATION MODEL

The model for terahertz radiation generation considered here assumes that the laser beams propagate in fully ionized

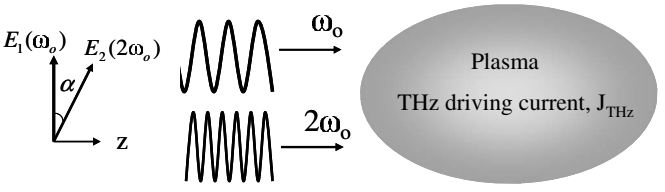

FIG. 1. Schematic of the two-color laser/plasma terahertz generation process. The fundamental (E_1) and the second harmonic (E_2) transversely polarized laser fields copropagating along the z axis in a fully ionized plasma. The fundamental frequency is ω_o and the angle between the polarizations is α.

air. In this section we determine the current density responsible for terahertz radiation making use of the one-dimensional, relativistic, cold fluid equations. The fundamental and the second harmonic laser fields are assumed to be copropagating and transversely polarized, with an angle α between their directions of polarization as shown schematically in Fig. 1. The fundamental frequency ω_o is assumed to be large compared with $1/\tau_L$, where τ_L is laser pulse duration. The coupling of the laser pulses generates a low-frequency ($\sim 1/\tau_L$) current density that can radiate in the terahertz regime for the parameters regime considered here. By solving the electron fluid equations to third order in the laser field amplitude we find that the terahertz driving current contains contributions from both relativistic and ponderomotive effects. However, we show that in the parameter regime $\omega_o \gg \nu > 1/\tau_L$, where ν is the electron collision frequency, the ponderomotive contribution to the driving current far exceeds the relativistic contribution and constitutes the main current density for radiation at terahertz frequencies.

A. Laser fields

The two laser pulses with frequencies ω_o and $2\omega_o$ propagating in the z direction are represented by the vector potential

$$\mathbf{A}(z,t) = (1/2)A_1(z,t)\exp[i\Psi_1(z,t)]\hat{\mathbf{e}}_1 + (1/2)A_2(z,t)\exp[i\Psi_2(z,t)]\hat{\mathbf{e}}_2 + \text{c.c.}, \quad (1)$$

where $\Psi_1 = k_1 z - \omega_o t$, $\Psi_2 = k_2 z - 2\omega_o t$, $k_1 = (\omega_o^2 - \omega_p^2)^{1/2}/c$, $k_2 = (4\omega_o^2 - \omega_p^2)^{1/2}/c$, $\omega_p = (4\pi e^2 n/m)^{1/2}$ is the plasma frequency, e is the magnitude of electronic charge, m is the electron mass, c is the speed of light, and n is the electron density. The transverse unit vectors $\hat{\mathbf{e}}_1$ and $\hat{\mathbf{e}}_2$ define the polarization of the laser pulses and the angle between the polarization vectors is α, i.e., $\hat{\mathbf{e}}_1 \cdot \hat{\mathbf{e}}_2 = \cos\alpha$. The laser envelopes A_1 and A_2 vary slowly in time and space compared to $1/\omega_o$ and c/ω_o, i.e., $\omega_o \gg 1/\tau_L$, where the laser pulse durations are assumed to be the same and equal to τ_L.

B. Terahertz driving current density

The transverse electron current density that drives the terahertz radiation, correct to third order in the laser field, is given by the low-frequency (dc) component of

$$\mathbf{J}_{\text{THz}} = \mathbf{J}_{\text{pond}} + \mathbf{J}_{\text{rel}}, \quad (2)$$

where $\mathbf{J}_{\text{pond}} = qn^{(2)}\mathbf{v}_\perp^{(1)}$ is due to electron density modulations arising from the ponderomotive force and $\mathbf{J}_{\text{rel}} = qn_o\mathbf{v}_\perp^{(3)}$ is due to relativistic effects. In these expressions n and $\mathbf{v}_\perp$ denote the electron density and transverse fluid velocity, respectively, the superscripts denote the order of the quantity with respect to the laser amplitude, and $q = -e$ is the signed electronic charge. In the present one-dimensional (1D) model there is no second-order transverse velocity or first-order electron density perturbation.

C. Electron fluid velocity

The relativistic momentum equation for the electron fluid is given by $d\mathbf{p}/dt + \nu\mathbf{p} = q(\mathbf{E} + \mathbf{v}\times\mathbf{B}/c)$, where $\mathbf{p} = \gamma m\mathbf{v}$, m is the electron mass, $\mathbf{v}$ is the electron fluid velocity, $\gamma = (1 - \mathbf{v}\cdot\mathbf{v}/c^2)^{-1/2}$, and ν is the electron collision frequency. We write the total electric and magnetic fields (due to the lasers and the plasma), in terms of the scalar and vector potentials, i.e., $\mathbf{E} = -\nabla\Phi - c^{-1}\partial\mathbf{A}/\partial t$ and $\mathbf{B} = \nabla\times\mathbf{A}$. Expanding the momentum equation to include contributions that are third order in the laser fields gives

$$\left(\frac{\partial}{\partial t} + \mathbf{v}\cdot\nabla + \nu\right)\mathbf{v} = -c^2\nabla\varphi - c\frac{\partial\mathbf{a}}{\partial t} + c\mathbf{v}\times(\nabla\times\mathbf{a}) + \frac{(\mathbf{v}\cdot\mathbf{v})}{2c}\frac{\partial\mathbf{a}}{\partial t} + \frac{\mathbf{v}}{c^2}\left(\mathbf{v}\cdot\frac{\partial\mathbf{v}}{\partial t}\right), \quad (3)$$

where, $\mathbf{a} = q\mathbf{A}/mc^2$ and $\varphi = q\Phi/mc^2$ are the normalized vector and scalar potentials. On the right side of Eq. (3), the first three terms represent the Lorentz force and the last two terms are relativistic contributions. The scalar potential, which results from the ponderomotively driven electron density perturbations, is second order in the laser fields. The transverse velocity, from Eq. (3), correct to third order in the laser fields, is written as $\mathbf{v}_\perp = \mathbf{v}_\perp^{(1)} + \mathbf{v}_\perp^{(3)}$. For a linearly polarized fundamental Gaussian laser beam with spot size r_L, $|\mathbf{a}| = 8.6\times10^{-10}\lambda[\mu\text{m}](I[\text{W/cm}^2])^{1/2}$ and the power is $P[GW] = 21.5(|\mathbf{a}|r_L/\lambda)^2$.

1. Current density due to ponderomotive effects

The first-order transverse velocity is given by $(\partial/\partial t + \nu)\mathbf{v}_\perp^{(1)} = -c\,\partial\mathbf{a}/\partial t$, whose solution, for $\omega_o \gg \nu, 1/\tau_L$, is

$$\mathbf{v}_\perp^{(1)} = -c(1 - i\nu/\omega_o)\mathbf{a}_1 - c(1 - i\nu/2\omega_o)\mathbf{a}_2. \quad (4)$$

The second-order electron density and axial electron velocity are given by $\partial n^{(2)}/\partial t + n_o\partial v_z^{(2)}/\partial z = 0$ and $\partial v_z^{(2)}/\partial t + \nu v_z^{(2)} = -c^2\partial\varphi/\partial z + c(\mathbf{v}_\perp^{(1)}\times\nabla\times\mathbf{a})_z$, respectively, where $\partial^2\varphi/\partial z^2 = -4\pi q^2 n^{(2)}/mc^2$. Combining these equations we obtain

$$\left(\frac{\partial^2}{\partial t^2} + \nu\frac{\partial}{\partial t} + \omega_p^2\right)n^{(2)} = \frac{n_o c^2}{2}\frac{\partial^2(\mathbf{a}\cdot\mathbf{a})}{\partial z^2}, \quad (5a)$$

$$\left(\frac{\partial^2}{\partial t^2} + \nu\frac{\partial}{\partial t} + \omega_p^2\right)v_z^{(2)} = -\frac{c^2}{2}\frac{\partial^2(\mathbf{a}\cdot\mathbf{a})}{\partial z\,\partial t}. \quad (5b)$$

The terahertz field is driven by the high frequency components of $\mathbf{a}\cdot\mathbf{a}$ at $2\omega_o$ and ω_o, i.e., $\mathbf{a}\cdot\mathbf{a} = (a_1^2/4)\exp(2i\Psi_1) + (a_1^* a_2/2)\cos\alpha\exp[i(\Psi_2 - \Psi_1)] + \text{c.c.}$ The solution of Eq. (5a), with the appropriate high frequency terms in $\mathbf{a}\cdot\mathbf{a}$ which drive the terahertz radiation, is

$$n^{(2)} = \frac{n_o c^2}{2}\left\{\frac{k_1^2 a_1^2\exp(2i\Psi_1)}{4\omega_o^2 + 2i\omega_o\nu - \omega_p^2} + \frac{(1/2)(k_2 - k_1)^2 a_1^* a_2\cos\alpha\exp[i(\Psi_2 - \Psi_1)]}{\omega_o^2 + i\omega_o\nu - \omega_p^2} + \text{c.c.}\right\}. \quad (6)$$

Combining Eqs. (4) and (6), the ponderomotive plasma current density for terahertz generation, $\mathbf{J}_{\rm pond}=qn^{(2)}\mathbf{v}_{\perp}^{(1)}$, is given by

$$\mathbf{J}_{\rm pond}=-\frac{qn_oc^3}{8}\left[\frac{(k_2-k_1)^2(1+i\nu/\omega_0)}{\omega_0^2+i\nu\omega_0-\omega_p^2}\cos\alpha\hat{\mathbf{e}}_1+\frac{2k_1^2(1-i\nu/2\omega_0)}{4\omega_0^2+2i\nu\omega_0-\omega_p^2}\hat{\mathbf{e}}_2\right](a_1^*)^2a_2\exp(i\Delta kz)+\text{c.c.},\tag{7}$$

where $\Delta k=k_2-2k_1=(3/4)(\omega_p/\omega_o)\omega_p/c$. In obtaining Δk, finite laser spot size effects are neglected since $\omega_p^2r_L^2/c^2\gg1$. In the regime where $\omega_o\gg(\nu,1/\tau_L)$ and $\omega_o\gg\omega_p$ the current density in Eq. (7) reduces to

$$\mathbf{J}_{\rm pond}=-\frac{qn_oc}{8}(a_1^*)^2a_2\exp(i\Delta kz)\hat{\mathbf{e}}_{\perp}+\text{c.c.},\tag{8}$$

where $\hat{\mathbf{e}}_{\perp}=\cos\alpha\hat{\mathbf{e}}_1+(1/2)\hat{\mathbf{e}}_2$.

2. Current density due to relativistic effects

The third order fluid velocity obtained from Eq. (3) is given by

$$\left(\frac{\partial}{\partial t}+\nu\right)\mathbf{v}_{\perp}^{(3)}=-v_z^{(2)}\left(c\frac{\partial\mathbf{a}}{\partial z}+\frac{\partial\mathbf{v}_{\perp}^{(1)}}{\partial z}\right)+\left(\frac{\mathbf{v}_{\perp}^{(1)}}{c}\cdot\frac{\partial\mathbf{a}}{\partial t}\right)\mathbf{v}_{\perp}^{(1)}+\frac{c}{2}\left(\frac{\mathbf{v}_{\perp}^{(1)}}{c}\cdot\frac{\mathbf{v}_{\perp}^{(1)}}{c}\right)\frac{\partial\mathbf{a}}{\partial t},\tag{9}$$

which for $\omega_o\gg\nu$ reduces to $(\partial/\partial t+\nu)\mathbf{v}_{\perp}^{(3)}=(c/2)\{\partial[(\mathbf{a}\cdot\mathbf{a})\mathbf{a}]/\partial t\}$. The terahertz plasma current density due to relativistic effects is $\mathbf{J}_{\rm rel}=qn_o\mathbf{v}_{\perp}^{(3)}$ and is given by

$$\mathbf{J}_{\rm rel}\approx\frac{qn_oc}{8(1+\nu\tau_L)}(a_1^*)^2a_2\exp(i\Delta kz)\hat{\mathbf{e}}_{\perp}+\text{c.c.},\tag{10}$$

where only terms that drive the terrahertz radiation are retained in $(\mathbf{a}\cdot\mathbf{a})\mathbf{a}$, i.e., $(\mathbf{a}\cdot\mathbf{a})\mathbf{a}=(1/4)(a_1^*)^2a_2\exp(i\Delta kz)\hat{\mathbf{e}}_{\perp}+\text{c.c.}$

D. Current density source for terahertz radiation

From Eqs. (2), (8), and (10) the total driving current for the terahertz radiation is

$$\mathbf{J}_{\rm THz}\approx-\frac{qn_oc}{8}\left(\frac{\nu\tau_L}{1+\nu\tau_L}\right)(a_1^*)^2a_2\exp(i\Delta kz)\hat{\mathbf{e}}_{\perp}+\text{c.c.}\tag{11}$$

In the absence of collisions $\mathbf{J}_{\rm pond}\approx-\mathbf{J}_{\rm rel}$ and the net current density that drives the terahertz radiation nearly vanishes. In the parameter regime $\nu\tau_L\gg1$, the ponderomotive current density far exceeds the relativistic current density, i.e., $\mathbf{J}_{\rm pond}\gg\mathbf{J}_{\rm rel}$ and the total driving current for the terahertz radiation is

$$\mathbf{J}_{\rm THz}\approx-\frac{qn_oc}{8}(a_1^*)^2a_2\exp(i\Delta kz)\hat{\mathbf{e}}_{\perp}+\text{c.c.}\tag{12}$$

For the parameters considered here, $\nu\tau_L>1$, as discussed in the following subsection.

The driving source for the terahertz radiation can be represented by a nonlinear polarization field $\mathbf{P}_{\rm THz}^{(3)}$ with a third order susceptibility $\chi^{(3)}$, where $\mathbf{P}_{\rm THz}^{(3)}=(i/\omega)\mathbf{J}_{\rm THz}=(1/4)\chi^{(3)}(E_1)^2E_2\hat{\mathbf{e}}_{\perp}$. Using Eq. (12) we find that

$$|\chi^{(3)}|=\frac{1}{16\sqrt{2}\pi}\left(\frac{\omega_p}{\omega_o}\right)^2\left(\frac{q\tau_L}{mc}\right)^2\frac{1}{\omega_o\tau_L}.\tag{13}$$

The susceptibility associated with the Kerr effect in neutral air (at STP) is $\chi_{Kerr}^{(3)}\approx1.2\times10^{-17}$ esu [23]. For picosecond laser pulses and fully ionized air, the susceptibility in Eq. (13) associated with the terahertz generation process considered here is comparable with $\chi_{Kerr}^{(3)}$. However, it should be noted that Eq. (13) applies to a plasma and therefore the process considered here has the potential to scale to high powers without the breakdown issues associated with air.

E. Electron collision frequency

The total electron collision frequency is the sum of the electron-ion and electron-neutral collision frequencies, $\nu=\nu_{ei}+\nu_{en}$ [24]. The electron-ion collision frequency is given by $\nu_{ei}[\text{s}^{-1}]\approx3\times10^{-6}(\ln\Lambda)n[\text{cm}^{-3}](W_e[\text{eV}])^{-3/2}\approx3\times10^{-5}n[\text{cm}^{-3}](W_e[\text{eV}])^{-3/2}$, where the gas is assumed to be singly ionized, we have taken $\ln\Lambda=10$, n is the electron density, $W_e\approx(W_{osc}^2+T_e^2)^{1/2}$, W_{osc} is the electron oscillation energy in the laser fields, and T_e is the electron temperature. The electron oscillation energy is $W_{osc}[\text{eV}]=m[qE_L/(2m\omega_o)]^2=9.35\times10^{-14}(\lambda[\mu\text{m}])^2I_L[\text{W/cm}^2]$, where $I_L=cE_L^2/(8\pi)$ is the laser intensity and $E_L[\text{V/cm}]=27.4(I_L[\text{W/cm}^2])^{1/2}$ (linear polarization) is the laser electric field. For the laser intensities considered here, $W_{osc}\gg T_e$. Furthermore, the plasma is not in local thermodynamic equilibrium (LTE) since the time required to reach LTE, $\tau_{\rm LTE}$, is much greater than the laser pulse duration, i.e., $\tau_{\rm LTE}>(M/m)\nu^{-1}\gg\tau_L$, where M is the molecular mass.

The electron-neutral collision frequency is $\nu_{en}[\text{s}^{-1}]\approx(n_n-n)\sigma_nv\approx2\times10^{-7}(n_n-n)[\text{cm}^{-3}](W_e[\text{eV}])^{1/2}$, where σ_n is the molecular cross-section, $n_n=2.7\times10^{19}$ cm^{-3} is the neutral

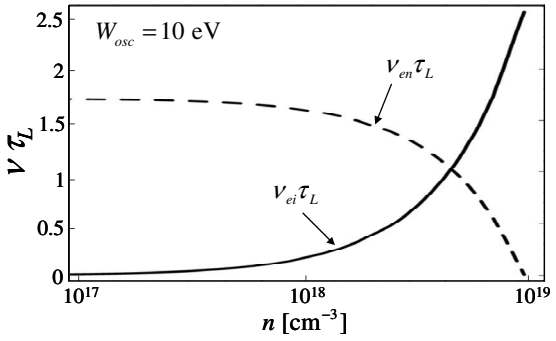

FIG. 2. Normalized electron collision frequency as a function of electron density in air. Solid dashed curve denotes electron-ion collision frequency, dashed curve denotes electron-neutral collision frequency. The ambient neutral density of air is taken to be $n_n=2.7\times10^{19}$ cm^{-3}. The electron oscillation energy, W_{osc}, in the field of the laser which has intensity $\sim10^{14}$ W/cm^2, is taken to be 10 eV ($\gg T_e$). Note that the plasma is not in LTE. In the examples in the text we assume a fully ionized plasma, hence, $\nu\tau_L>1$.

density of air and v is the electron velocity. The electron-ion and electron-neutral collision frequencies are plotted in Fig. 2 as a function of electron density. An electron oscillation energy of 10 eV has been assumed in the presence of a laser field of intensity 10^{14} W/cm^2. For a wide range of electron density, the electron collision frequency, $\nu > 1/\tau_L$. In the examples that follow, we assume that the plasma is fully ionized, and for simplicity, use Eq. (12) for the terahertz current source.

III. TERAHERTZ RADIATION ENERGY SPECTRUM IN THE FAR FIELD

The terahertz driving current, Eq. (12), can be expressed in the form

$$\mathbf{J}_{\mathrm{THz}}(x,y,z,t) = \hat{J}_{\mathrm{THz}}\sigma(x,y)\cos(\Delta k z + \Delta\theta)\Theta(L_0/2 - |z|) \times \exp[-(t - z/V_g)^2/\tau_L^2]\hat{\mathbf{e}}_\perp, \tag{14}$$

where $\hat{J}_{\mathrm{THz}} = (qn_o c/4)|(a_1^*)^2 a_2|$, $\sigma(x,y)$ characterizes the transverse profile, $\Theta(x)$ is the Heaviside function, L_o is the interaction length, V_g is the group velocity and $\Delta\theta$ is the phase. In the representation for the current the two-color lasers are taken to be overlapping, having a Gaussian profile with pulse duration τ_L.

The interaction length is determined by a number of factors, including the diffraction of the fundamental wavelength laser pulse and group velocity slippage of the fundamental relative to the second harmonic. The group velocity of the fundamental and 2nd harmonic in plasma, normalized to c is approximately $\beta_{g(0,2)} \approx c[1 + \omega_p^2/(2\omega_{0,2}^2)]^{-1}$, where the subscripts (0, 2) denote the fundamental and second harmonic, respectively. The slippage-limited interaction length is $L_{0,slip} \approx c\tau_L/(\beta_{g2} - \beta_{g0})$. The actual interaction length is the smaller of $L_{0,slip}$ and the Rayleigh length of the fundamental, $Z_{R1} = \pi r_L^2/\lambda_1$, where r_L is the laser spot size and λ_1 is the fundamental wavelength.

A. Terahertz field

The terahertz field is given by $(\nabla^2 - c^{-2}\partial^2/\partial t^2)\mathbf{E} = 4\pi c^{-2}\partial \mathbf{J}_{\mathrm{THz}}/\partial t$, which has the exact solution

$$E(x,y,z,t) = -\frac{1}{c^2}\int_{-\infty}^{\infty} dx_o \int_{-\infty}^{\infty} dy_o \int_{-\infty}^{\infty} dz_o \times \frac{(\partial/\partial t)J_{\mathrm{THz}}(x_o,y_o,z_o,t - \bar{R}/c)}{\bar{R}}, \tag{15}$$

where $\mathbf{E} = E\hat{\mathbf{e}}_\perp$, $\mathbf{J}_{\mathrm{THz}} = J_{\mathrm{THz}}\hat{\mathbf{e}}_\perp$ and $\bar{R} = [(x - x_o)^2 + (y - y_o)^2 + (z - z_o)^2]^{1/2}$. The Fourier transform of the terahertz field, defined by $\hat{E}(x,y,z,\omega) = (2\pi)^{-1/2}\int_{-\infty}^{\infty} dt E(x,y,z,t)\exp(i\omega t)$, is

$$\hat{E}(x,y,z,\omega) = \frac{i}{\sqrt{2}}\frac{\hat{J}_{\mathrm{THz}}}{c^2}\frac{\exp[i(\omega/c)R]}{R}(\omega\tau_L)\exp(-\omega^2\tau_L^2/4) \times \int_{-\infty}^{\infty} dx_o \int_{-\infty}^{\infty} dy_o \int_{-\infty}^{\infty} dz_o \sigma(x_o,y_o)h(z_o) \times \cos(\Delta k z_o + \Delta\theta)$$

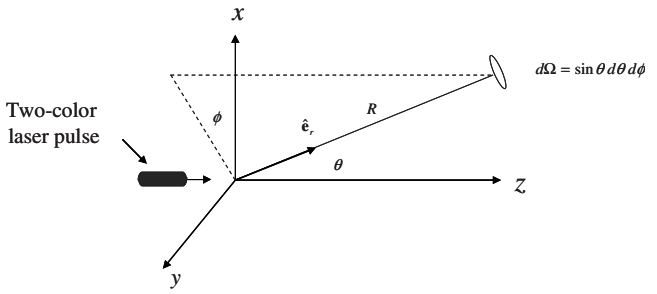

FIG. 3. Two-color laser pulse propagating along the z axis. The Cartesian coordinate system and the spherical polar coordinate system used in calculating the terahertz radiation characteristics in the far field are indicated.

$$\times \exp\left\{-i\frac{\omega}{cR}[xx_o + yy_o + (z - cR/V_g)z_o\right\}, \tag{16}$$

where $R = (x^2 + y^2 + z^2)^{1/2}$, and we have used the relation

$$\int_{-\infty}^{\infty} d\tau \exp(i\omega\tau)\exp(-\tau^2/\tau_L^2) = \sqrt{\pi}\tau_L \exp(-\omega^2\tau_L^2/4),$$

together with the far field expansion $\bar{R} \approx R[1 - (xx_o + yy_o + zz_o)/R^2]$. The far field limit is defined by, $R \gg L_o, c\tau_L, r_o$ where r_o is the characteristic transverse dimension of the terahertz current density. The transverse dimension of the plasma generated by ionization of air is typically less than the laser spot size.

To obtain the spectral and angular characteristics of the terahertz radiation in the far field limit we use spherical coordinates (R, θ, ϕ). Figure 3 shows the two-color laser pulses together with the coordinate system used in the far field calculation. The transformation between coordinates is given by $x = R\sin\theta\cos\phi$, $y = R\sin\theta\sin\phi$, $z = R\cos\theta$. The polarization of the two laser pulses determines the polarization of the terahertz field through the driving current. The angular dependence of the terahertz radiation field is with respect to the polarization of the driving current which we have arbitrarily chosen to be in the y direction, hence, $E_R = E_y \sin\theta\sin\phi$, $E_\theta = E_y\cos\theta\sin\phi$ and $E_\phi = E_y\cos\phi$.

The Fourier transform of the electric field in Eq. (16), in spherical coordinates, is

$$\hat{E} = \frac{\hat{J}_{\mathrm{THz}}V_o}{\sqrt{2}c^2}\left\{\frac{\exp[i(\omega/c)R]}{R}\right\}G(\theta,\omega), \tag{17}$$

where

$$G(\theta,\omega) = \left\{\frac{J_1[(\omega/c)r_o\sin\theta]}{(\omega/c)r_o\sin\theta}\right\}H(\theta,\omega)(\omega\tau_L)\exp(-\omega^2\tau_L^2/4), \tag{18}$$

$$H(\theta,\omega) = \frac{2i}{L_o}\int_{-\infty}^{\infty} dz_o h(z_o) \times \cos(\Delta k z_o)\exp[-i(\omega/c)(\cos\theta - c/V_g)z_o] = i\left\{\frac{\sin[(\omega-\omega_R)\tau_o]}{(\omega-\omega_R)\tau_o} + \frac{\sin[(\omega+\omega_R)\tau_o]}{(\omega+\omega_R)\tau_o}\right\}, \quad (19)$$

$\omega_R(\theta)=\Delta kc(\beta_g^{-1}-\cos\theta)^{-1}$, $\tau_o(\theta)=(\beta_g^{-1}-\cos\theta)L_o/(2c)$, $V_o=\pi r_o^2 L_o$ is the volume of the source and we have set $\Delta\theta=0$. In obtaining Eq. (17) the following relation was used

$$\int_{-\infty}^{\infty} dx_o \int_{-\infty}^{\infty} dy_o \sigma(x_o,y_o)\exp[-i(\omega/c)(x_o\sin\theta\cos\phi + y_o\sin\theta\sin\phi)] = 2\pi r_o^2 \frac{J_1[(\omega/c)r_o\sin\theta]}{(\omega/c)r_o\sin\theta},$$

where $\sigma=1$, for $\rho_o \le r_o$ and 0 otherwise.

In general, the directionality of terahertz emission depends strongly on the assumed parameters, for example, plasma density, pulse duration, and laser wavelength. In what follows, we calculate the emitted radiation in the time domain for the particular case of an ultrashort laser pulse with $\lambda=0.8$ μm, $\tau_L \sim 100$ fs, and its second harmonic propagating in fully ionized air.

The function $G(\theta,\omega)$ is largest for frequencies $\omega \sim 1/\tau_L$. Hence, for angles $(r_o/c\tau_L)\sin\theta \ll 1$, i.e., in the near-forward and near-backward directions, we can set $J_1[(\omega/c)r_o\sin\theta]/[(\omega/c)r_o\sin\theta] \approx 1/2$ and analytically evaluate the time-domain terahertz field writing Eq. (17) as

$$E(t) \approx \frac{E_0}{2}\int_{-\infty}^{\infty} \frac{d(\omega\tau_L)}{\sqrt{2\pi}}\exp[i\omega(t-R/c)]H(\theta,\omega)(\omega\tau_L) \times \exp(-\omega^2\tau_L^2/4), \quad (20)$$

for angles $\theta \approx (0,\pi)$, where $E_0 \equiv \hat{J}_{\mathrm{THz}}V_0/(\sqrt{2}Rc^2\tau_L)$.

Forward terahertz field ($\theta \approx 0$). In the near-forward direction, we can assume that $\omega \sim 1/\tau_L \ll \omega_R$ for $\beta_g \approx 1$ and approximate Eq. (19) as $H(\theta\approx 0,\omega) \approx 2i\sin(\omega_R\tau_o)\cos(\omega\tau_o)/(\omega_R\tau_o)$.

The time-domain terahertz field in the near-forward direction is then given by

$$E(t) \approx \sqrt{2}E_0\frac{\sin(\Delta kL_0/2)}{\Delta kL_0/2}[(\bar{\tau}_R-\bar{\tau}_o)e^{-(\bar{\tau}_R-\bar{\tau}_0)^2} + (\bar{\tau}_R+\bar{\tau}_o)e^{-(\bar{\tau}_R+\bar{\tau}_o)^2}], \quad (21)$$

where $\bar{\tau}_R=\tau_R/\tau_L$, $\tau_R=(t-R/c)$ is the retarded time, and $\bar{\tau}_o=\tau_o/\tau_L$. The forward-directed field is characterized by two single-cycle pulses, each with duration $\sim\tau_L$ and separation $2\tau_o$. The pulses result from the interaction of the drive laser pulses with the plasma gradient in the front and back of the interaction region. For $\tau_o \ll \tau_L$, the terahertz field is a single-cycle pulse given by

$$E(t) \approx 2\sqrt{2}E_0\frac{\sin(\Delta kL_0/2)}{\Delta kL_0/2}\bar{\tau}_R e^{-\bar{\tau}_R^2}. \quad (22)$$

Backward terahertz field ($\theta \approx \pi$). In the backward direction, $\omega_R \approx \Delta kc/2$. For typical parameters, e.g., a 100 fs laser pulse propagating in fully ionized air, $\omega_R \approx 1/\tau_L$, and $f_R=\omega_R/(2\pi)\approx 2.1$ THz. If the length of the interaction region is long compared to the pulse length ($L_0 \gg c\tau_L$), the integrand of Eq. (20) is sharply peaked about frequencies $\omega=\pm\omega_R$. In this case, we can approximately integrate Eq. (20) giving

$$E(t) \approx \sqrt{2\pi}E_0(\omega_R\tau_L)\left(\frac{\tau_L}{2\tau_o}\right)\exp[-(\omega_R\tau_L)^2/4] \times \sin(\omega_R\tau_R)\Theta(\tau_o-|\tau_R|). \quad (23)$$

The backward terahertz pulse has a duration $\sim L_0/c$ and a frequency $\omega_R \approx \Delta kc/2$.

B. Terahertz energy

The total terahertz energy radiated is $W_{\mathrm{THz}}=\int_{-\infty}^{\infty}dt\int \mathbf{S}\cdot d\mathbf{A}$, where $\mathbf{S}=c\mathbf{E}\times\mathbf{B}/4\pi$ is the Poynting flux and $d\mathbf{A}=R^2\sin\theta d\theta d\phi\hat{\mathbf{e}}_R=R^2 d\Omega\hat{\mathbf{e}}_R$ is the differential area in a plane perpendicular to the unit radial vector, $\hat{\mathbf{e}}_R=\sin\theta\cos\phi\hat{\mathbf{e}}_x+\sin\theta\sin\phi\hat{\mathbf{e}}_y+\cos\theta\hat{\mathbf{e}}_z$, and $d\Omega=\sin\theta d\theta d\phi$. The total radiated terahertz energy can be written as

$$W_{\mathrm{THz}} = R^2\int_\Omega d\Omega\int_{-\infty}^{\infty} dt(\mathbf{S}\cdot\hat{\mathbf{e}}_R). \quad (24)$$

The radial component of the Poynting flux integrated over all time is

$$\int_{-\infty}^{\infty} dt(\mathbf{S}\cdot\hat{\mathbf{e}}_R) = i\frac{c^2}{4\pi}\int_0^{\infty}\frac{d\omega}{\omega}(\hat{\mathbf{E}}\times\boldsymbol{\nabla}\times\hat{\mathbf{E}}^* - \hat{\mathbf{E}}^*\times\boldsymbol{\nabla}\times\hat{\mathbf{E}})\cdot\hat{\mathbf{e}}_R = \frac{c}{2\pi}p(\alpha)h(\theta,\phi)\int_0^{\infty} d\omega\hat{E}\hat{E}^*, \quad (25)$$

where $h(\theta,\phi)=(1-\sin^2\theta\sin^2\phi)$ and

$$p(\alpha) = 2\cos^2\alpha + 1/4. \quad (26)$$

The total terahertz energy radiated can be written as

$$W_{\mathrm{THz}} = \int_\Omega d\Omega\int_0^{\infty} d\omega\frac{\partial^2\tilde{\tilde{W}}_{\mathrm{THz}}}{\partial\omega\,\partial\Omega} = \int_0^{\infty} d\Omega\frac{\partial\tilde{W}_{\mathrm{THz}}}{\partial\Omega}, \quad (27)$$

where $\partial^2\tilde{\tilde{W}}_{\mathrm{THz}}/\partial\omega\partial\Omega$ is the total energy per solid angle per frequency interval and $\partial\tilde{W}_{\mathrm{THz}}/\partial\Omega$ is the total energy per unit solid angle. Comparing Eq. (24) with Eq. (27) and using Eq. (25) we find

$$\frac{\partial^2\tilde{\tilde{W}}_{\mathrm{THz}}}{\partial\omega\,\partial\Omega} = \frac{cR^2}{2\pi}p(\alpha)h(\theta,\phi)\hat{E}\hat{E}^* = \frac{(\hat{J}_{\mathrm{THz}}V_o)^2}{4\pi c^3\tau_L}p(\alpha)\tilde{\tilde{f}}(\theta,\phi,\omega), \quad (28)$$

where $\tilde{\tilde{f}}(\theta,\varphi,\omega)=\tau_L h(\theta,\phi)|G(\theta,\omega)|^2$ characterizes the angular and frequency dependence, and $\hat{J}_{\mathrm{THz}}$ is proportional to the plasma density and scales with laser intensity as $I_1\sqrt{I_2}$. The polarization function $p(\alpha)$ is maximum for $\alpha=0$, i.e., when the lasers are aligned.

The amplitude of $\partial^2\tilde{\tilde{W}}_{\mathrm{THz}}/\partial\omega\partial\Omega$ is large when $\omega_R\tau_L\approx 1$ and $\omega_R r_0/c\leq 1$, i.e., for backward emission ($\theta>\pi/2$). Additionally, for interaction lengths $L_0\gg(r_0,c\tau_L)$, the function $\partial^2\tilde{\tilde{W}}_{\mathrm{THz}}/\partial\omega\partial\Omega$ is sharply peaked about frequencies $\pm\omega_R$. Hence, in this parameter regime, the frequency integration in Eq. (27) can be carried out approximately to give

$$\frac{\partial\tilde{W}_{\mathrm{THz}}}{\partial\Omega}\approx\frac{(\hat{J}_{\mathrm{THz}}V_o)^2}{2c^3}\frac{\omega_R}{\Delta kL_0}p(\alpha)h(\theta,\phi)\left|\left\{\frac{J_1[(\omega_R/c)r_o\sin\theta]}{(\omega_R/c)r_o\sin\theta}\right\}\times(\omega_R\tau_L)\exp(-\omega_R^2\tau_L^2/4)\right|^2, \quad (29)$$

where it was assumed that $\Delta kL_0\gg 1$.

The spectral distribution function integrated over all solid angles is $W_{\mathrm{THz}}=p(\alpha)\eta_o W_o(a_1^2a_2)^2$, where $W_o=(\hat{J}_{\mathrm{THz}}V_o)^2/(4\pi c^3\tau_L)=(qN_e)^2/(64\pi c\tau_L)$, $N_e=n_o(\pi r_L^2L_o)$, $\eta_o=\tau_L\int d\omega d\Omega h(\theta,\phi)|G(\theta,\omega)|^2$, $a_{1,2}=8.6\times10^{-10}\lambda_{1,2}[\mu\mathrm{m}](I_{1,2}[\mathrm{W/cm^2}])^{1/2}$ and $\lambda_{1,2}=\lambda_o,\lambda_o/2$. The total terahertz energy in practical units can be written as

$$W_{\mathrm{THz}}[pJ]=3\times10^{-10}p(\alpha)\eta_0(n_e/n_n)^2\frac{r_o^4L_o^2}{\tau_L}\lambda_1^6I_1^2I_2. \quad (30)$$

where r_o and λ_1 are in units of microns, L_o is in centimeters, τ_L in picoseconds, and I_1 and I_2 are in $\mathrm{TW/cm^2}$. For typical experimental parameters, the total radiated terahertz energy according to Eq. (30) is on the order of multiple picoJoules, as discussed in the following section.

IV. DISCUSSION

The four-wave mixing process considered here for terahertz generation has a number of characteristics that can be compared with experiments. From Eq. (28) we note that (1) the total terahertz energy is proportional to $I_1^2I_2$, i.e., the terahertz field amplitude is proportional to $I_1\sqrt{I_2}$ and (2) the terahertz emission is maximized when the polarization of the laser beams and the terahertz are aligned [Eq. (26)]. Both of these features are in agreement with experimental observations [9].

To quantify the theoretical predictions, we consider terahertz generation in fully ionized air at atmospheric pressure. The fundamental wavelength is $\lambda_o=0.8$ μm. The laser intensities are assumed to be equal, $I_1=I_2=2\times10^{14}$ $\mathrm{W/cm^2}$ ($a_1=10^{-2}$, $a_2=0.5\times10^{-2}$), the laser pulse durations are $\tau_L=100$ fs ($c\tau_L=30$ μm), and the laser spot sizes are $r_L=40$ μm. The group velocity of the fundamental laser pulse is $\sim0.992c$. The group velocity slippage length of the fundamental relative to the second harmonic is $L_{0,slip}\approx0.5$ cm, which is comparable to the Rayleigh length, $\pi r_L^2/\lambda_0\approx0.6$ cm. In the examples that follow, we assume an interaction length $L_0=0.5$ cm. The radius of the terahertz current is taken to be $r_o=15$ μm. The interaction volume is $V_o=\pi r_o^2L_o\approx3.3\times10^{-6}$ $\mathrm{cm^3}$. For these parameters, the number of electrons in the interaction volume is $N_e=n_o\pi r_L^2L_o\approx10^{14}$, $W_o=(qN_e)^2/(64\pi c\tau_L)\approx0.4$ k J, and $\eta_0\approx10^{-2}$. The total terahertz energy radiated according to Eq. (30) is $W_{\mathrm{THz}}\approx2$ pJ.

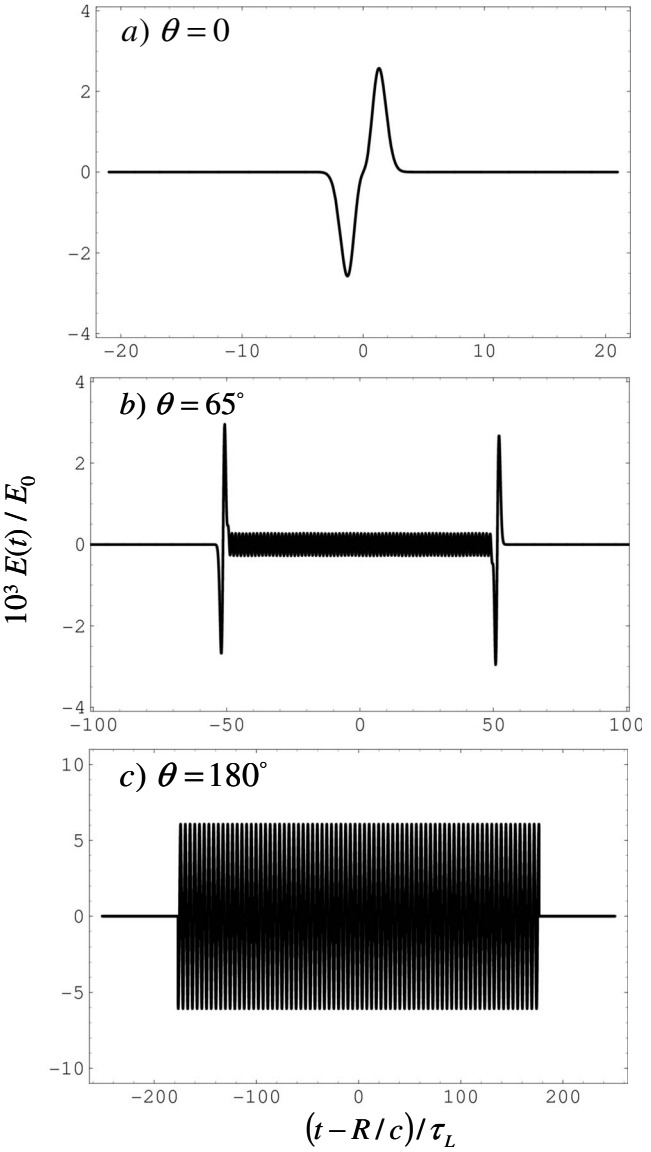

FIG. 4. Terahertz electric field obtained by inverse Fourier transform of Eq. (17) for parameters $n_0=2.7\times10^{19}$ $\mathrm{cm^{-3}}$, $\lambda_o=0.8$ μm, $I_1=I_2=2\times10^{14}$ $\mathrm{W/cm^2}$, $\tau_L=100$ fs, $r_L=40$ μm, $r_o=14$ μm, $R=1$ m, $V_g/c=0.992$, $L_0=0.5$ cm. The field is normalized to $E_0=\hat{J}_{\mathrm{THz}}V_0/(\sqrt{2}Rc^2\tau_L)$ and plotted as a function of normalized delayed time $(t-R/c)/\tau_L$ for angles (a) $\theta=0$, (b) $\theta=65°$, and (c) $\theta=180°$. For these parameters, $E_0\approx8.3$ MV/cm.

The normalized time-domain terahertz electric field in various directions is plotted in Fig. 4. For these parameters, $E_0=[2\pi\eta_0/(c\tau_L)]^{1/2}/R\approx8.3$ MV/cm at a distance of $R=1$ m. The field profile in the forward direction is characterized by a single-cycle pulse with duration of order $\sim\tau_L$ with an amplitude of ~20 kV/cm. In the backward direction, the terahertz pulse has duration $\sim360\tau_L$ and frequency $f_R=\omega_R/(2\pi)\approx2.1$ THz. In both the forward and backward directions, the analytic expressions for the terahertz field, i.e., Eqs. (21) and (23) are in excellent agreement with the

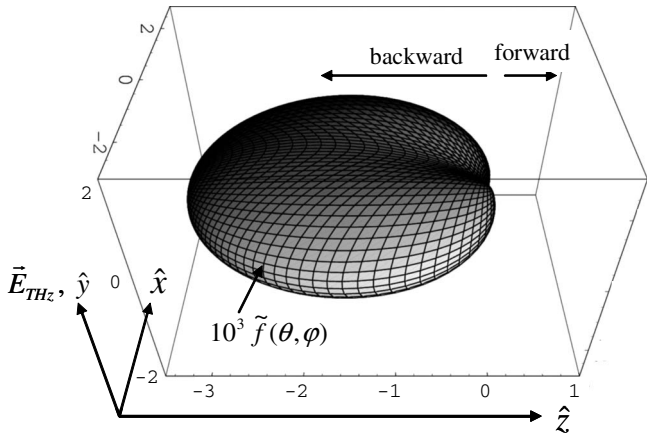

FIG. 5. Spherical polar plot of $\tilde{f}(\theta,\phi)=\tau_L\int_0^\infty h(\theta,\phi)|G(\theta,\omega)|^2 d\omega$, i.e., the normalized energy per unit solid angle. The angles θ and ϕ are defined in Fig. 2. The radial extent of the surface denotes the magnitude of $10^3\tilde{f}$ in the direction (θ,φ). The terahertz electric field is polarized in the y direction. Parameters are the same as for Fig. 4.

numerical inverse Fourier transform of Eq. (17) for these parameters. Figure 4(b) plots the laterally emitted terahertz field at an angle ~65°, obtained by numerical inverse Fourier transform of Eq. (17). The field is characterized by a pulse of duration $\sim 100\tau_L$ with large-amplitude, single-cycle structures at the leading and trailing edges. The single-cycle structures result from the interaction of the drive lasers with the plasma gradients at the front and back of the interaction region.

Figure 5 shows the spatial distribution of the emitted terahertz energy integrated over all frequencies, i.e., $\tilde{f}(\theta,\phi)=\tau_L\int_0^\infty h(\theta,\phi)|G(\theta,\omega)|^2 d\omega$. The radial extent of the surface in a given direction (θ,ϕ) represents the amplitude of $\tilde{f}$. The surface is slightly flatter in direction of polarization of the terahertz field. The emitted terahertz energy is largest in the backward direction. The amplitude of the forward-emitted terahertz is not visible on the plotted scale.

Figure 6 shows the spatial distribution of terahertz energy integrated over azimuthal angle, i.e., $g(\theta)=\int_0^{2\pi}\tilde{f}(\theta,\phi)d\varphi$.

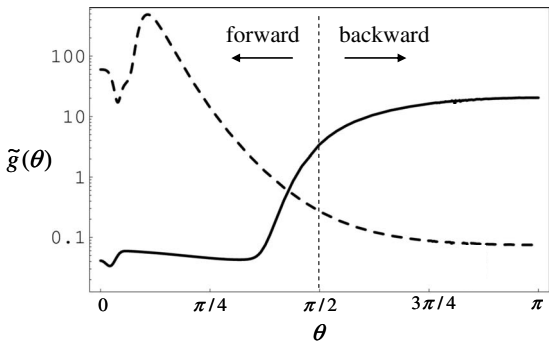

FIG. 6. Normalized terahertz amplitude function, integrated over azimuthal angle and frequency, i.e., $\tilde{g}(\theta)\equiv 10^3\int_0^{2\pi}\tilde{f}d\varphi$, plotted as a function of angle θ. Curves correspond to fully ionized air (solid curve), and partially ionized air ($n=10^{18}$ cm^{-3}, dashed curve). Other parameters are the same as for Fig. 4.

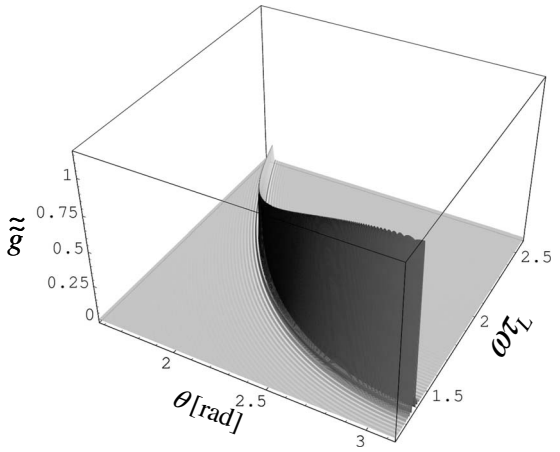

FIG. 7. Normalized terahertz amplitude function integrated over azimuthal angle, i.e., $\tilde{\tilde{g}}(\theta,\omega)\equiv\int_0^{2\pi}\tilde{\tilde{f}}d\varphi$, plotted as a function of normalized frequency, $\omega\tau_L$, and angle, θ. Parameters are the same as for Fig. 4.

Terahertz energy emitted in the backward direction is more than two orders of magnitude larger than in the forward direction. The parameters are the same as in Fig. 4.

Figure 7 plots the terahertz amplitude function $\tilde{\tilde{f}}$ integrated over azimuthal angle, ϕ, as a function of normalized frequency, $\omega\tau_L$, and angle, θ. The terahertz emission spectrum in the backward direction is sharply peaked at frequency $\omega\tau_L\approx 1.3$, i.e., ~2.1 THz. The central terahertz frequency increases and emission amplitude decreases as θ decreases.

Finally, we note that the direction of terahertz emission is a sensitive function of the assumed parameters. For example, if the air is not fully ionized and the plasma density is assumed to be $\sim 10^{18}$ cm^{-3}, the direction of radiation is primarily within a small-angle cone in the forward direction, as indicated by the dashed curve in Fig. 6.

V. SUMMARY

We have presented a theoretical model for terahertz generation based on four-wave mixing of fundamental and second harmonic ultrashort laser pulses in collisional plasma. The model reproduces a number of properties of terahertz radiation observed in recent experiments [9]. For example, the terahertz field amplitude is proportional to $I_1\sqrt{I_2}$, the terahertz emission is maximized when the polarization of the laser beams and the terahertz are aligned. The emitted terahertz field in the forward direction is on the order of tens of kV/cm and is characterized by an approximately single-cycle pulse with duration comparable to that of the drive laser pulses. In addition, the model also predicts that for the assumed parameters, e.g., fully ionized air, the terahertz energy emitted in the backward direction (relative to the propagation of the drive laser pulses) is orders of magnitude larger than in the forward direction and contains many oscillations at frequency $\approx 1/\tau_L$(~2.1 THz).

The terahertz generation process can be can be represented by a nonlinear polarization field with a third-order

susceptibility. The relativistic and ponderomotive contributions to the susceptibility nearly cancel in the absence of electron collisions. Therefore, in this terahertz generation mechanism, collisional effects play a critical role. For picosecond laser pulses and fully ionized air, the nonlinear susceptibility associated with the terahertz generation process is comparable with the nonlinear Kerr index of air. However, it should be noted that the nonlinear susceptibility calculated here applies to plasma, so that this process has the potential to scale to high powers without the breakdown issues associated with air.

ACKNOWLEDGMENTS

The authors thank Dr. K.Y. Kim, Dr. H. Milchberg, and Dr. A. Zigler for useful discussions on this topic. This work was supported by 6.1 funding from the Office of Naval Research.

[1] P. H. Siegel, IEEE Trans. Microwave Theory Tech. **50**, 910 (2002).
[2] D. M. Mittleman, R. H. Jacobsen, and M. C. Nuss, IEEE J. Sel. Top. Quantum Electron. **2**, 679 (1996).
[3] H. Hamster, A. Sullivan, S. Gordon, and R. W. Falcone, Phys. Rev. E **49**, 671 (1994).
[4] D. J. Cook and R. M. Hochstrasser, Opt. Lett. **25**, 1210 (2000).
[5] M. Kress, T. Löffler, S. Eden, M. Thomson, and H. G. Roskos, Opt. Lett. **29**, 1120 (2004).
[6] T. Löffler, M. Kress, M. Thomson, and H. G. Roskos, Acta Phys. Pol. A **107**, 99 (2005).
[7] N. Karpowicz and X. C. Zhang, Phys. Rev. Lett. **102**, 093001 (2009).
[8] X. G. Dong, Z. M. Sheng, H. C. Wu, W. M. Wang, and J. Zhang, Phys. Rev. E **79**, 046411 (2009).
[9] X. Xie, J. Dai, and X. C. Zhang, Phys. Rev. Lett. **96**, 075005 (2006).
[10] K. Y. Kim, J. H. Glownia, A. J. Taylor, and G. Rodriguez, Opt. Express **15**, 4577 (2007).
[11] K. Y. Kim, A. J. Taylor, J. H. Glownia, and G. Rodriguez, Nat. Photonics **2**, 605 (2008).
[12] V. B. Gildenburg and N. V. Vvedenskii, Phys. Rev. Lett. **98**, 245002 (2007).
[13] W. P. Leemans, C. G. R. Geddes, J. Faure, Cs. Tóth, J. van Tilborg, C. B. Schroeder, E. Esarey, G. Fubiani, D. Auerbach, B. Marcelis, M. A. Carnahan, R. A. Kaindl, J. Byrd, and M. C. Martin, Phys. Rev. Lett. **91**, 074802 (2003).
[14] C. D'Amico, A. Houard, M. Franco, B. Prade, A. Mysyrowicz, A. Couairon, and V. T. Tikhonchuk, Phys. Rev. Lett. **98**, 235002 (2007).
[15] P. Sprangle, J. R. Peñano, B. Hafizi, and C. A. Kapetanakos, Phys. Rev. E **69**, 066415 (2004).
[16] T. Bartel, P. Gaal, K. Reimann, M. Woerner, and T. Elsaesser, Opt. Lett. **30**, 2805 (2005).
[17] W. Hoyer, A. Knorr, J. V. Moloney, E. M. Wright, M. Kira, and S. W. Koch, Phys. Rev. Lett. **94**, 115004 (2005).
[18] N. A. Yampolsky and G. M. Fraiman, Phys. Plasmas **13**, 113108 (2006).
[19] E. Esarey, P. Sprangle, B. Hafizi, and P. Serafim, Phys. Rev. E **53**, 6419 (1996).
[20] D. Hashimshony, A. Zigler, and K. Papadopoulos, Phys. Rev. Lett. **86**, 2806 (2001).
[21] M. Yu. Glyavin, A. G. Luchinin, and G. Yu. Golubiatnikov, Phys. Rev. Lett. **100**, 015101 (2008).
[22] A. Fliflet, M. Hornstein, and S. Gold, *Design of a Multi-kW, 600 GHz, Second-Harmonic Gyrotron*, Digest of Conference Papers of the 33rd International Conference on Infrared, Millimeter and Terahertz Waves, (unpublished).
[23] R. W. Boyd, *Nonlinear Optics*, 2nd ed. (Academic, San Diego, CA, 2003), Table 4.1.2.
[24] *NRL Plasma Formulary*, edited by J. D. Huba (U.S. GPO, Washington, D.C., 2006).